Characterization of a Lewis adduct in its inner and outer forms

Wei-Chun Liu[1]*†, François P. Gabbaï[1]*‡

[1]Department of Chemistry, College Station, Texas 77843-3255, US

*Corresponding author. Email: francois@tamu.edu

Abstract: The entrance channel of bimolecular reactions sometimes involves the formation of outer complexes as weakly bound, fleeting intermediates. Here, we characterize such an outer complex in a system that models the bimolecular, C-O bond-forming reaction of a phosphine oxide Lewis base with a carbenium Lewis acid. Crystallographic studies show that the C-O distance in the outer form exceeds that of the final or inner adduct by 1.1 Å. As the system samples the two forms of the complex, which correspond to minima on the corresponding potential energy surface, the C-O linkage switches from a secondary interaction in the outer complex to a dative bond in the inner complex. This phenomenon is harnessed as a functional feature to stabilize xanthylium-based photoredox catalysts.

Pre-reactive complexes held by weak intermolecular forces are sometimes present on the potential energy surfaces of bimolecular reactions (*1-3*). Consideration of these fleeting intermediates, which have been inferred from kinetic (*4, 5*) or spectroscopic experiments (*6, 7*), may be traced back to the pioneering work of Mulliken, who suggested their existence in simple reactions such as those leading to Lewis adducts (*8*). Mulliken, who referred to these pre-reactive complexes as outer complexes, explained, based on resonance theory, that they differ from the corresponding inner complexes or classical Lewis adducts, by the extent of charge transfer from the Lewis base to the Lewis acid. In all cases, the involvement of a pre-reactive or outer complex will give rise to a double-well on the potential energy surface of the corresponding reaction (Fig. 1A) (*8*).

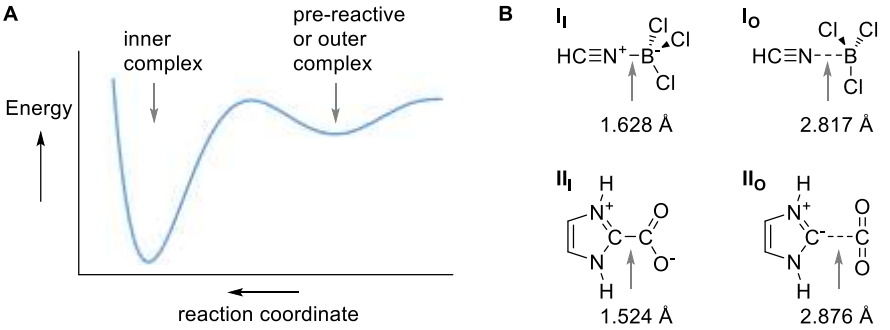

Fig. 1. Background and conceptual overview (**A**) Idealized potential energy surface of a bimolecular Lewis acid-base reaction, with minima corresponding to the outer and inner complexes. (**B**) Examples of model Lewis acid-base systems computed to involve outer complexes as stationary points on the potential energy surface of the Lewis adduct forming reaction.

The relevance of Mulliken's early analyses has resurfaced in the structural chemistry of nitrile-borane adducts (*9, 10*). For example, the simple adduct CH_3CN-BF_3 forms a short B-N bond of 1.630(4) Å in the solid state (*9*), but its characterization in the gas phase returns a much longer distance of 2.011(7) Å for the same linkage (*11*). Calculations performed on this system led to the proposed involvement of an outer complex that rapidly exchanges in the gas phase with its inner counterpart (*12*). These computational results are corroborated by a recent *in silico* investigation of HCN-BCl_3 (**I**), which also features two minima at B-N distances of 1.628 Å for the outer complex **I**$_O$ and 2.817 Å for the inner complex **I**$_I$ (Fig. 1B) (*13, 14*). Despite the widely different distances and bonding modes, the stabilities of these two isomers differ by less than 1 kcal/mol even as the bond transitions from a polar covalent bond in the inner form of the adduct to a π-hole-based triel bond in outer form (*13*). A related situation is predicted in the case of adducts formed by the coordination of *N*-heterocyclic carbenes to CO_2. For example, the NHC-CO_2 system (**II**, NHC = $C(NHCH)_2$) was calculated to feature two minima characterized by C_{NHC}-C_{CO_2} distances of 1.524 Å for **II**$_I$ and 2.876 Å for **II**$_O$ (Fig. 1B) (*15*). Bonding analysis of **II**$_O$ points to the presence of a C_{NHC}-C_{CO_2} secondary interaction, referred to as a tetrel bond (*16-19*). This designation refers to a non-covalent and, thus, elongated bonding mode in which electrostatic forces and second-order donor-acceptor bonding constitute the major terms stabilizing the linkage (*20*). The picture that emerges from Mulliken's early work and more recent investigations of simple Lewis adducts is one in which a weakly bound outer complex

serves as an entrance channel for the more robust, datively bonded inner complex. Frustrated Lewis pair systems (*21, 22*) where a datively bonded Lewis adduct is in equilibrium with a frustrated encounter complex (*23-26*) embodies another version of Mulliken early analyses even if, in this case, the outer or encounter complex features a long separation and no direct bonding interaction between the Lewis opposite atoms (*27, 28*).

As noted by Mulliken and Person, inner and outer complexes are isomers of one another, which differ by the distance separating the Lewis acid from the base (*29*). Despite the body of experimental and theoretical evidence gathered to date, examples of systems where both the inner and outer isomers of an adduct are structurally characterized have remained elusive. Motivated by the structural and electronic versatility that such an isomerism may provide, we have actively been searching for molecular designs that would support the concomitant existence of the two forms of a Lewis adduct. Here, we report an intramolecular example of such a system involving a phosphine oxide as the Lewis base and a carbenium ion as the Lewis acid. We were prompted to investigate such systems by prior reports on reversible dative bonding in intramolecular phosphine oxide-borane (*30-32*) and phosphine-carbenium adducts (*26*).

Synthesis and characterization of the inner and outer isomers

Access to our target system began with the synthesis of phosphine **1**, which was obtained by mono-lithiation of 1,8-dibromo-acenaphthene followed by reaction with (p-$ClC_6H_4)_2PCl$ (Fig. 2A). Subsequent lithiation of **1** followed by reaction with xanthone produced carbinol **2** which was converted in the phosphine oxide carbenium species [**3**][BF_4] by reaction with hydrogen peroxide and tetrafluoroboric acid. NMR analysis of [**3**][BF_4] in d_3-MeCN points to the presence of a P=O---C_{carb} interaction as indicated by the ^{13}C NMR chemical shift of the carbenium nucleus at 156.1 pm. Indeed, this chemical shift is almost 20 ppm upfield from the value of 176.1 ppm measured in the same solvent for the 9-phenylxanthylium cation ([^{Ph}**Xt**]$^+$), which features an uncompromised, Lewis-base-free, carbenium center. At the same time, the chemical shift of [**3**][BF_4] is 68.5 ppm downfield from that of the isopropyl phosphine oxide analog [**4**][BF_4] (87.6 ppm in $CDCl_3$), which was prepared for comparative purposes using a similar route. We also noted a difference in the behavior of these two compounds. Whereas [**4**][BF_4] is colorless both in the solid state and in solution, solid [**3**][BF_4] assumes a pinkish hue. When dissolved in CH_2Cl_2, it displays a reddish color associated with an absorption band at λ_{max} = 520 nm, suggesting that the xanthylium chromophore becomes at least partially unmasked (Fig. 2B).

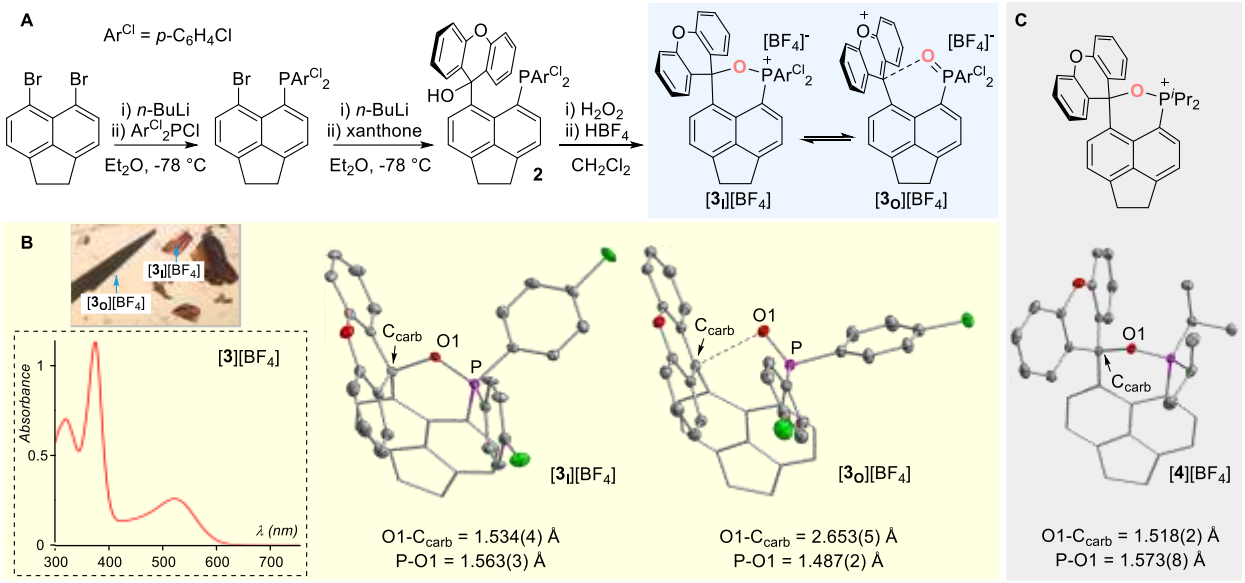

Fig. 2. Synthesis and characterization. (**A**) Synthesis of [**3**][BF_4]. (**B**) Photograph of crystals of [**3**][BF_4] showing specimens of different colors and morphologies, UV-vis spectrum of [**3**][BF_4] in CH_2Cl_2, and crystal structures of the inner ([**3I**][BF_4]) and outer ([**3O**][BF_4]) forms of [**3**][BF_4]. (**C**) Representation and crystal structure of [**4**][BF_4]. For all crystal structures shown, the thermal ellipsoids in the structures are drawn at the 50% probability level. Hydrogen atoms, counter anions, and interstitial solvent molecules were omitted for clarity.

To shed light on these results, we attempted to crystallize both [**3**][BF_4] and [**4**][BF_4]. Crystals of [**4**][BF_4] could be easily obtained (Fig. 2C). Their analysis using single crystal x-ray diffraction shows the collapse of the phosphine oxide functionality onto the xanthylium unit, leading to a tetracoordinate C_{carb} center with a C_{carb}-O1 bond distance of 1.518(2) Å. The formation of this bond leads to a P-O1 bond of 1.573(8) Å, distinctly longer than that of $^tBu_2PhPO$ (1.49 Å) (*33*). This lengthening, which illustrates substantial activation of the PO bond, indicates that [**4**][BF_4] is best described as an alkoxyphosphonium derivative. Having confirmed the formation of a short C_{carb}-O1 bond in the case of [**4**][BF_4], we turned our attention to [**3**][BF_4], which, as explained above, presented a somewhat ambiguous behavior. Crystallizing this derivative from CH_2Cl_2/Et_2O (1:10 vol.) afforded colorless crystals of the salt, which, based on an x-ray diffraction structural assay, feature the alkoxy phosphonium form of cation $[\mathbf{3}]^+$, with a short C_{carb}-O1 of 1.534(4) Å. This form of the cation, referred to as $[\mathbf{3I}]^+$, adopts a structure similar to that of $[\mathbf{4}]^+$, with the phosphine oxide tightly bound to the former carbenium unit. This analogy extends to the P1-O1 bond, which, with a length of 1.563(3) Å, is also activated when compared to a simple phosphine oxide such as Ph_3PO (1.489 (2) Å) (*34*). Interestingly, when [**3**][BF_4] is crystallized from pure THF, deep brown crystals are also obtained in addition to colorless ones, the latter corresponding to [**3I**][BF_4] (Fig. 2C). Analysis of the brown crystals indicates that they contain the phosphine oxide/xanthylium or outer form of $[\mathbf{3}]^+$, referred to as $[\mathbf{3O}]^+$ (Fig. 2C). The tetrafluoroborate salt of this new isomer features a non-interacting, interstitial molecule of THF in its asymmetric unit. THF, being more polar than Et_2O, may favor nucleation and crystallization of the more polar outer isomer ($\mu_{calc.}$ = 10.3 D for $[\mathbf{3O}]^+$ vs. 6.4 for $[\mathbf{3i}]^+$). This argument is supported by prior studies documenting the role of solvent polarity in promoting the dissociation of phosphine oxide-borane adducts (*30, 31*).

Inspecting the structure of $[\mathbf{3_O}]^+$ reveals additional singularities. The distance separating the carbenium center from the phosphine oxide oxygen atom stands at 2.653(5) Å and thus exceeds that of $[\mathbf{3_I}]^+$ by over 1 Å. At the same time, this distance is well within the sum of the van der Waals radii of the two elements (3.22 Å) (*35*), pointing to the presence of a secondary bonding interaction. Of note also is the trigonal planar geometry of the carbenium center, indicating that the carbenium center C_{carb} is not compromised through formation of a primary polar covalent interaction with the phosphine oxide as in the case of $[\mathbf{3_I}]^+$. The fact that isomers $[\mathbf{3_I}]^+$ and $[\mathbf{3_O}]^+$ differ by the length of the C_{carb}-O1 bond leads us to propose that they may be referred to as valence tautomers (*36-38*) or bond-stretch isomers (*39, 40*) of one another, with the former nomenclature being favored since formation of the C_{carb}-O1 single bond in $[\mathbf{3_I}]^+$ is accompanied by a decrease in the PO bond order. While C-O bond isomerism such as that encountered in $[\mathbf{3}]^+$ has not been previously studied either experimentally or *in silico*, a comparison with HCN-BCl_3 (**I**) (*13*) and NHC-CO_2 (**II**) was considered using the formal shortness ratio (FSR) (*41*) as a metric that accounts for the inherent difference in the covalent radii of the constituent atoms. This analysis shows that the FSR of inner (FSR = 1.08 for $[\mathbf{3_I}]^+$, 1.05 for $\mathbf{I_I}$, and 1.05 for $\mathbf{II_I}$) or outer forms (FSR$_\mathbf{O}$ = 1.80 for $[\mathbf{3_O}]^+$, 1.82 for and $\mathbf{I_O}$, and 1.97 for and $\mathbf{II_O}$) of the three systems are comparable. The analogous behavior of these systems is important because both a tethered system, such as $[\mathbf{3}]^+$, and untethered ones such as **I** and **II,** behave similarly.

Computational modeling

Further insights into the bonding of $[\mathbf{3_I}]^+$ and $[\mathbf{3_O}]^+$ were derived from computations. Optimization of the structures of these two isomers was carried out at the B97M-V/def2-mTZVP level of theory affording computed C_{carb}-O1 distances of 1.54 Å for $[\mathbf{3_I}]^+$ and 2.65 Å $[\mathbf{3_O}]^+$, in good agreement with the experimental values (1.534(4) Å for $[\mathbf{3_I}]^+$ and 2.653(5) Å $[\mathbf{3_O}]^+$). With these optimized structures at our disposal, we carried out an atoms-in-molecules (AIM) analysis (*42*), which unveiled, in both cases, a bond path connecting the carbenium center to the oxygen of the phosphine oxide moiety (Fig. 3A). The elevated electron density ($\rho(r)$) value of 1.96×10^{-1} in the $[\mathbf{3_I}]^+$ is consistent with the formation of a bond displaying significant covalency, which is also supported by the negative values of both the Hessian H(r) (-2.06×10^{-1}) and Laplacian $\nabla^2\rho(r)$ (-2.62×10^{-1}) (*43*). By contrast, the low $\rho(r)$ value of 2.34×10^{-2} e/Å^3 determined for $[\mathbf{3_O}]^+$ indicates the presence of a weaker interaction. This $\rho(r)$ value is comparable to that found for the long C-N interaction in IM-F_2CO, a species that has been described as the tetrel-bonded adduct of imidazole and F_2CO (Fig. 3A) (*44*). The sign and magnitude of the Hessian and Laplacian are also comparable ($H(r) = 0.917\times10^{-3}$ and $\nabla^2\rho(r) = 0.751\times10^{-1}$ for $[\mathbf{3_O}]^+$ *vs* $H(r) = 0.3\times10^{-3}$ and $\nabla^2\rho(r) = 0.65\times10^{-1}$ for IM-F_2CO), leading to propose that the C_{carb}-O1 interaction in $[\mathbf{3_I}]^+$ is a tetrel bond. To solidify this view, we have also carried out second-order perturbation theory calculations using the Natural Bond Orbital (NBO) program (Fig. 3A). This approach reveals that the C_{carb}-O1 bond in $[\mathbf{3_O}]^+$ corresponds to a second-order donor-acceptor interaction involving an oxygen lone pair as the donor and the carbenium p orbital as the acceptor. This interaction, which can be regarded as the orbital term of the C_{carb}-O1 tetrel bond, makes a significant contribution of 27.3 kJ/mol (E_{del}) to the stability of the molecule. The coulombic term of this interaction can be qualitatively derived from an inspection of the Electrostatic Potential (ESP) map depicted in Fig. 3B. This map shows a π-hole located over the carbenium atom (*45*), interacting with the negative surface presented by the oxygen atom of the phosphine oxide unit. This situation, described for other tetrel-bonded systems (*17-19*), indicates electrostatic attraction between the Lewis opposite partners. In the case of $[\mathbf{3_I}]^+$, the NBO

analysis identifies an NLMO (Natural Localized Molecular Orbital) that spans the two atoms. The atomic parentage of this NLMO (O 72.1%, C 27.9%) confirms the polar covalent or dative nature of the interaction.

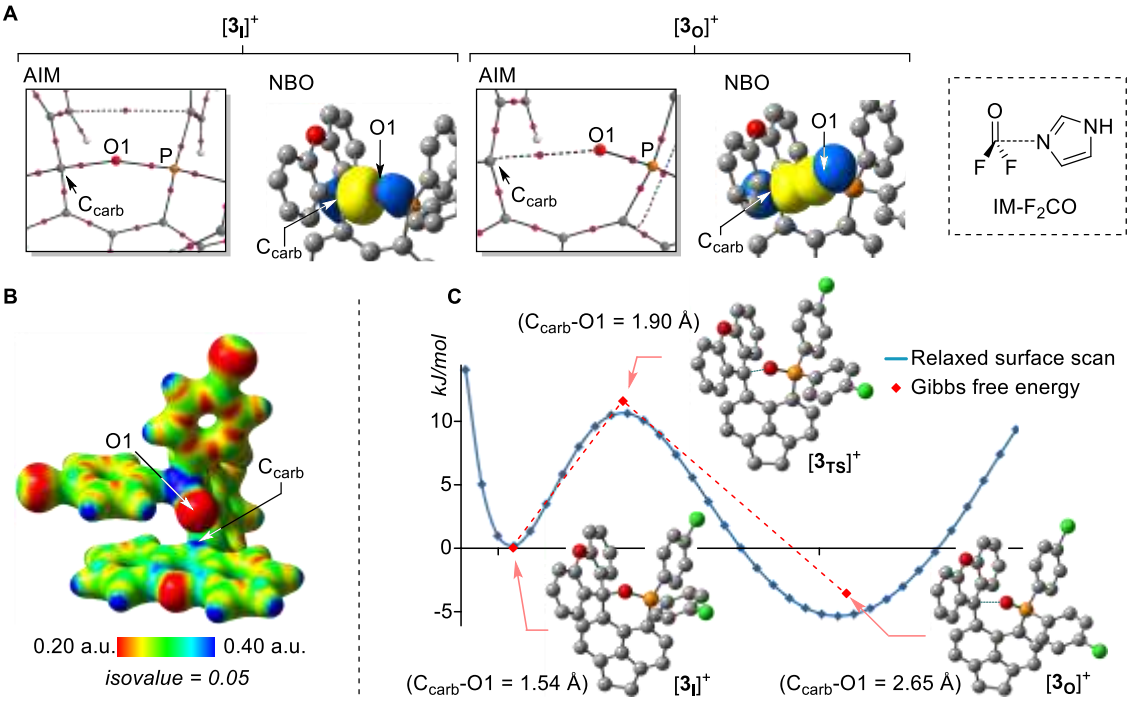

Fig. 3. Computational investigation of [3]$^+$. (**A**) AIM and NBO plots obtained for [**3I**]$^+$ and [**3O**]$^+$. The plots have been truncated to focus on the C_{carb}-O1 linkage. The AIM plots show the bond paths connecting the two atoms while the NBO plots show the relevant orbitals. The structure of IM-F_2CO is also shown as an inset. (**B**) ESP map of [**3I**]$^+$ plotted with an isovalue of 0.05. (**C**) Relaxed potential surface scan of [**3**]$^+$ upon elongation of the C_{carb}-O1 distance from 1.4 Å to 3.0 Å, showing the existence of two energy minima (blue data point and solid line). The optimized structure of [**3I**]$^+$, [**3TS**]$^+$ and [**3O**]$^+$ are also shown, along with their Gibbs free energy (red data point and dashed line).

Having established the nature of the bonding in [**3I**]$^+$ and [**3O**]$^+$, we next aimed to confirm that these two isomers correspond to minima on the potential energy surface of the molecule (*39, 40*). This view is readily confirmed by a scan of the potential energy surface of the molecule as a function of the C_{carb}-O1 bond length. Indeed, this scan affords two minima at 1.55 Å and 2.55 Å, separated by only 5.4 kJ/mol in favor of the outer isomer (Fig. 3B). The geometry of each minimum was further optimized at the B97M-V/def2-mTZVP level of theory, resulting in structures identical to those obtained when starting from the x-ray coordinates. To disambiguate the role played by the supporting backbone which may be viewed as structurally enforcing the outer isomer, we also carried out computations on the [Me_3PO-CPh_3]$^+$ model system. A scan of the potential energy surface of this unsupported model system upon incremental elongation of the C_{carb}-O bond also affords a double-well potential allowing us to conclude that the observation of an inner and outer form of [**3**]$^+$ is not an artifact imposed by the acenaphthene backbone. We note, however, that the second minimum of [Me_3PO-CPh_3]$^+$ occurs at a longer distance (2.80 Å) than in [**3**]$^+$ (2.55 Å), underpinning the structural assistance of the intramolecular design adopted for [**3**]$^+$. The transition state [**3TS**]$^+$ connecting these two minima displays an imaginary

frequency associated to the stretch of the C_{carb}-O1, completing our characterization of this double-well potential energy surface. With a value of 10.2 kJ/mol, the barrier separating these two minima is shallow, suggesting that both the inner and outer isomers rapidly interconvert. Such an observation appears inconsistent with our ability to observe both isomers experimentally. However, this incongruence can be reconciled by invoking the large lattice forces, which elevate this barrier, allowing for the trapping of either isomer. Indeed, an estimation of the lattice energy using CrystalExplorer(*46*) affords values of 612.0 and 587.1 kJ/mol for [**3I**][BF_4] and [**3O**][BF_4]THF, respectively. Energy decomposition analysis shows that the coulombic and dispersion terms contribute almost equally to the stability of the lattice, which is further strengthened by, albeit weaker, polarization interactions (see SM). We propose that these large lattice energies contribute to freezing the inner and outer forms of [**3**][BF_4] in their respective structures. Efforts to observe the isomerization of [**3I**][BF_4] into the outer form in the solid only led to the melting of [3I][BF4] above 240°C as confirmed by differential scanning calorimerty (DSC) and powder x-ray diffraction (see SM).

Solution behavior and photoredox catalysis

We have carried out variable-temperature $^{13}C\{^1H\}$ NMR measurements to verify that the two isomers are in fast equilibrium. Using a ^{13}C-enriched version of [**3**][BF_4] prepared for the purpose of this study, we observed a moderate shift of the resonance assigned to the carbenium center from 155.8 ppm at -35 ºC to 156.2 ppm at 50 ºC. Based on the assumption that the carbenium center chemical shift of [**3I**]$^+$ is identical to that of [**4**]$^+$ (88 ppm) while that [**3O**]$^+$ is identical to that of [^{Ph}**Xt**]$^+$ (176 ppm), fitting of the data to the van 't Hoff equation affords ΔH_{exp} = 0.21 ± 0.03 kJ/mol (R^2 = 0.96)which is close to the enthalpy difference derived from computation (ΔH_{calc} = 0.34 kJ/mol). In the context of these variable temperature measurements, we also synthesized the diphenylphosphine oxide analog [**5**][BF_4] and subjected it to the same $^{13}C\{^1H\}$ VT NMR experiment. The ^{13}C resonance assigned to the carbenium center of this derivative shows a more pronounced temperature dependence, progressively shifting from 104 ppm at -35 ºC to 114 ppm at 50 ºC, suggesting a larger enthalpy difference between the inner and outer isomers. Indeed, a van 't Hoff analysis of the experimental data affords ΔH_{exp} = 4.89 ± 0.08 kJ/mol (R^2 = 0.99), which is close to the computed value (ΔH_{calc} = 3.35 kJ/mol). We note in passing that only crystals of the inner isomer of [**5**][BF_4], namely [**5I**][BF_4], could be reproducibly obtained (see Supplementary Materials). Monitoring the P-O stretch of [**3**][BF_4] and [**5**][BF_4] by infrared spectroscopy in MeCN confirms the presence of the two equilibrating isomers characterized by a stretching frequency (ν_{PO}) in the 1110-1130 cm^{-1} range for the outer isomer while the inner form is detected in the 940-980 cm^{-1} range. [**4**][BF_4] which only exists in the inner form gives rise to ν_{PO} = 973 cm^{-1} while Ph_3PO with ν_{PO} = 1115 cm^{-1} serves as a good reference for [**3O**][BF_4] and [**5O**][BF_4]. The dynamic nature of the P=O-C_{carb} motif observed for [**3**][BF_4] and [**5**][BF_4] bears precedence in the behavior of phosphine oxide-borane intramolecular adducts that have also been shown to possess dynamic P=O-B motifs (*30, 32*).

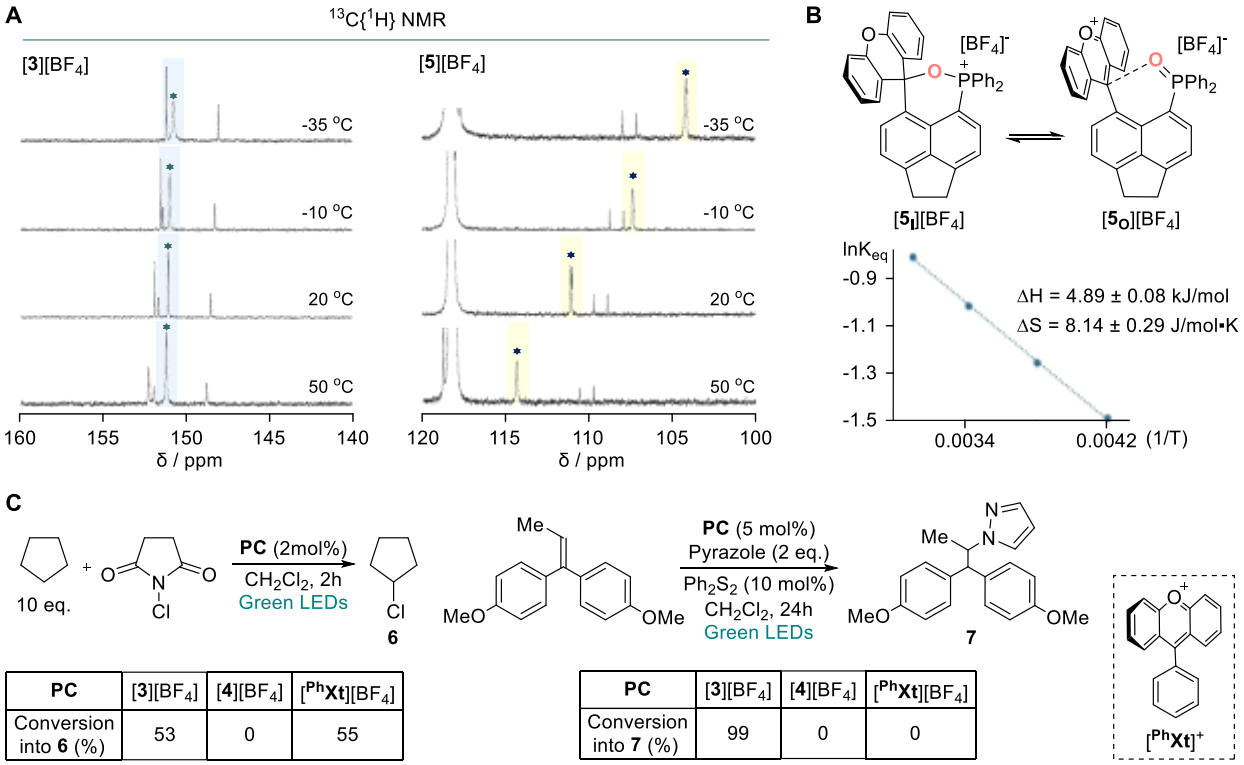

PC	[3][BF4]	[4][BF4]	[PhXt][BF4]
Conversion into **6** (%)	53	0	55

PC	[3][BF4]	[4][BF4]	[PhXt][BF4]
Conversion into **7** (%)	99	0	0

Fig. 4. Spectroscopic probing of interconversion dynamics and reactivity. (**A**) Portion of the $^{13}C\{^1H\}$ NMR spectra of [**3**][BF_4] and [**5**][BF_4] in solvent showing the effect of temperature on the ^{13}C resonance of the carbenium center. (**B**) Van 't Hoff analysis of the data obtained for [**5**][BF_4] with the corresponding equilibrium equation between the two isomers and the resulting thermodynamical parameters. (**C**) Reactions used to test the activity of [**3**][BF_4], [**4**][BF_4] and [^{Ph}**Xt**][BF_4] as photoredox catalysts. All reactions were carried out under green light irradiation and the conversions are derived from ^1H NMR spectroscopy. The inset shows the structure of [^{Ph}**Xt**]$^+$.

Aiming to turn the bistability of [**3**][BF_4] into a functional feature, we decided to test its capacity to serve as a photoredox catalyst. We were prompted to pursue this possibility by recent reports which demonstrated that xanthylium and thioxanthylium cations are efficient photocatalysts (*47-49*). As a prelude to these studies, we inspected the nature of the excited state of [**3**][BF_4] associated to the UV-vis band at λ_{max} = 520 nm. Time-dependent DFT calculations suggest that this feature belongs to [**3o**]$^+$ and corresponds to a transition from the acenaphthene-based HOMO to the xanthylium-centered LUMO. In turn, the resulting charge-separated excited state resembles that of acridinium-based photocatalysts such as Fukuzumi's catalysts (*50-52*). Calculation of the excited state oxidation potential using the reduction potential of [**3**][BF_4] ($E_{1/2}$ = -0.117 vs SCE) and its fluorescence spectrum (see SM) afforded a value of +2.03 V, which suggested that [**3**][BF_4] could function as an oxidation photocatalyst. This hypothesis was tested in the chlorination of cyclopentene using *N*-chlorosuccinimide and green light illumination. With a catalyst loading of 2 mol%, the reaction proceeded swiftly, affording chlorocyclopentene in 53% yield after 2 hours. When the same reaction was repeated with [**4**][BF_4], no conversion was observed, in line with the inability of [**4**]$^+$ to access its outer isomer. We also tested [^{Ph}**Xt**][BF_4] as a photocatalyst and found this simple xanthylium cation to have a comparable

activity. These initial results and comparison suggest that the activity of $[\mathbf{3}]^+$ arises from the capacity of this system to access the outer isomer $[\mathbf{3_O}]^+$, with the xanthylium moiety disengaged from dative bonding with the phosphine oxide moiety. We also tested the potential of $[\mathbf{3}][BF_4]$ to promote the addition of pyrazole to styrene, a reaction previously reported to proceed with 9-mesityl acridinium as the photoredox catalyst (*53*). We found that this reaction was also promoted by $[\mathbf{3}][BF_4]$ under green light irradiation, reaching completion after 24 h when a 5 mol% catalyst loading was employed. As in the chlorination reactions discussed above, $[\mathbf{4}][BF_4]$ was entirely inactive, leading us to again assign the photocatalytic properties of $[\mathbf{3}]^+$ to its outer isomer. Finally, we also endeavored to test $[^{\mathbf{Ph}}\mathbf{Xt}][BF_4]$ which proved to be entirely inactive in the same reaction under the same conditions. The failure of $[^{\mathbf{Ph}}\mathbf{Xt}]^+$ to promote this reaction is proposed to result from the reactivity of the carbenium center of this derivative under basic conditions, an interpretation consistent with the rapid discoloration of the catalyst solution when pyrazole is added. Such a decomposition is prevented in $[\mathbf{3}][BF_4]$ by the phosphine oxide functionality which reversibly masks the carbenium center.

Ongoing efforts in our laboratory aim to further develop the range of dative motifs that can also display the type of bistability observed in $[\mathbf{3}]^+$. Our efforts to diversify and generalize this phenomenon not only stem from our desire to build on these original findings but also to exploit the phenomenon beyond simple photocatalysis. We contemplate the possibility that the structural bistability of these systems may provide access to switchable Lewis acid and Lewis base chemistry with applications in the development of optoelectronic materials, catalysts, and platforms for small molecule activation.

References and Notes

Acknowledgments: All calculations were conducted with the advanced computing resources provided by Texas A&M High Performance Research Computing. We thank Dr. Donald Darensbourg for donating a sample of $^{13}CO_2$, Dr. Joseph Reibenspies for his help in collecting powder x-ray data and Dr. Peiran Wei for his help with DSC measurements.

Funding: We acknowledge generous support from the National Science Foundation (CHE-2154972), the Welch Foundation (A-1423), and Texas A&M University (Arthur E. Martell Chair of Chemistry).

Author contributions:

Conceptualization: WCL, FPG

Methodology: WCL

Investigation: WCL

Visualization: WCL, FPG

Funding acquisition: FPG

Supervision: FPG

Writing – original draft: WCL, FPG

Writing – review & editing: FPG, WCL

Data and materials availability: Crystallographic data have been deposited with the Cambridge Crystallographic Data Centre as supplementary publication no. CCDC 2345150-2340153. These data can be obtained free of charge via www.ccdc.cam.ac.uk/data_request/cif. All other data are available in the main text or the supplementary materials.

Supplementary Materials

Materials and Methods

Supplementary Text

Figs. S1 to S58

Tables S1 to S10

References (*46, 54-70*)

1. A. C. Legon, Prereactive Complexes of Dihalogens XY with Lewis Bases B in the Gas Phase: A Systematic Case for the Halogen Analogue B···XY of the Hydrogen Bond B···HX. *Angew. Chem. Int. Ed.* **38**, 2686-2714 (1999).
2. S. V. Rosokha, J. K. Kochi, The Preorganization Step in Organic Reaction Mechanisms. Charge-Transfer Complexes as Precursors to Electrophilic Aromatic Substitutions. *J. Org. Chem.* **67**, 1727-1737 (2002).
3. N. M. Donahue, Reaction Barriers: Origin and Evolution. *Chem. Rev.* **103**, 4593-4604 (2003).
4. J. I. Brauman, Some historical background on the double-well potential model. *J. Mass Spectrom.* **30**, 1649-1651 (1995).
5. H. Song, H. Guo, Theoretical Insights into the Dynamics of Gas-Phase Bimolecular Reactions with Submerged Barriers. *ACS Phys. Chem. Au.* **3**, 406-418 (2023).
6. D. M. Neumark, Spectroscopy of reactive potential energy surfaces. *PhysChemComm* **5**, 76-81 (2002).
7. A. C. Legon, Pre-reactive intermediates in gas-phase chemical reactions: a contribution from rotational spectroscopy. *Chem. Commun.*, 109-116 (1996).
8. R. S. Mulliken, Molecular Compounds and their Spectra. III. The Interaction of Electron Donors and Acceptors. *J. Phys. Chem.* **56**, 801-822 (1952).
9. B. Swanson, D. F. Shriver, J. A. Ibers, Nature of the donor-acceptor bond in acetonitrile-boron trihalides. The structures of the boron trifluoride and boron trichloride complexes of acetonitrile. *Inorg. Chem.* **8**, 2182-2189 (1969).
10. J. P. Wrass, D. Sadowsky, K. M. Bloomgren, C. J. Cramer, J. A. Phillips, Quantum chemical and matrix-IR characterization of $CH_3CN–BCl_3$: a complex with two distinct minima along the B–N bond potential. *Phys. Chem. Chem. Phys.* **16**, 16480-16491 (2014).
11. M. A. Dvorak, R. S. Ford, R. D. Suenram, F. J. Lovas, K. R. Leopold, van der Waals vs. covalent bonding: microwave characterization of a structurally intermediate case. *J. Am. Chem. Soc.* **114**, 108-115 (1992).
12. D. J. Giesen, J. A. Phillips, Structure, Bonding, and Vibrational Frequencies of $CH_3CN{-}BF_3$: New Insight into Medium Effects and the Discrepancy between the Experimental and Theoretical Geometries. *J. Phys. Chem. A* **107**, 4009-4018 (2003).

13. S. J. Grabowski, The Nature of Triel Bonds, a Case of B and Al Centres Bonded with Electron Rich Sites. *Molecules* **25**, 2703 (2020).
14. S. J. Grabowski, Two faces of triel bonds in boron trihalide complexes. *J. Comput. Chem.* **39**, 472-480 (2018).
15. J. E. Del Bene, I. Alkorta, J. Elguero, Carbenes as Electron-Pair Donors To CO2 for C···C Tetrel Bonds and C–C Covalent Bonds. *J. Phys. Chem. A* **121**, 4039-4047 (2017).
16. A. Bauzá, T. J. Mooibroek, A. Frontera, Tetrel-Bonding Interaction: Rediscovered Supramolecular Force? *Angew. Chem. Int. Ed.* **52**, 12317-12321 (2013).
17. A. Karim *et al.*, Carbon's Three-Center, Four-Electron Tetrel Bond, Treated Experimentally. *J. Am. Chem. Soc.* **140**, 17571-17579 (2018).
18. W.-C. Liu, Y. Kim, F. P. Gabbaï, Conformational Switching through the One-Electron Reduction of an Acridinium-based, γ-Cationic Phosphine Gold Complex. *Chem. Eur. J.* **27**, 6701-6705 (2021).
19. E. D. Litle, F. P. Gabbaï, Double axial stabilization of a carbenium ion via convergent P=O→C^+ tetrel bonding. *Chem. Commun.* **60**, 690-693 (2024).
20. L. M. Azofra, S. Scheiner, Tetrel, chalcogen, and CH··O hydrogen bonds in complexes pairing carbonyl-containing molecules with 1, 2, and 3 molecules of CO_2. *J. Chem. Phys.* **142**, 034307 (2015).
21. D. W. Stephan, Frustrated Lewis Pairs. *J. Am. Chem. Soc.* **137**, 10018-10032 (2015).
22. D. W. Stephan, G. Erker, Frustrated Lewis Pair Chemistry: Development and Perspectives. *Angew. Chem. Int. Ed.* **54**, 6400-6441 (2015).
23. S. J. Geier, D. W. Stephan, Lutidine/$B(C_6F_5)_3$: At the Boundary of Classical and Frustrated Lewis Pair Reactivity. *J. Am. Chem. Soc.* **131**, 3476-3477 (2009).
24. P. Spies *et al.*, Rapid intramolecular heterolytic dihydrogen activation by a four-membered heterocyclic phosphane–borane adduct. *Chem. Commun.*, 5072-5074 (2007).
25. L. J. Hounjet *et al.*, Combinations of Ethers and $B(C_6F_5)_3$ Function as Hydrogenation Catalysts. *Angew. Chem. Int. Ed.* **52**, 7492-7495 (2013).
26. A. C. Shaikh, J. M. Veleta, J. Moutet, T. L. Gianetti, Trioxatriangulenium ($TOTA^+$) as a Robust Carbon-based Lewis Acid in Frustrated Lewis Pair Chemistry. *Chem. Sci.* **12**, 4841-4849 (2021).
27. G. Erős *et al.*, Expanding the Scope of Metal-Free Catalytic Hydrogenation through Frustrated Lewis Pair Design. *Angew. Chem. Int. Ed.* **49**, 6559-6563 (2010).
28. T. C. Johnstone, G. N. J. H. Wee, D. W. Stephan, Accessing Frustrated Lewis Pair Chemistry from a Spectroscopically Stable and Classical Lewis Acid-Base Adduct. *Angew. Chem. Int. Ed.* **57**, 5881-5884 (2018).
29. R. S. Mulliken, W. B. Person, *Molecular Complexes*. (John Wiley & Sons, Inc., New York, 1969), pp. 498.
30. Y. Cao, J. K. Nagle, M. O. Wolf, B. O. Patrick, Tunable Luminescence of Bithiophene-Based Flexible Lewis Pairs. *J. Am. Chem. Soc.* **137**, 4888-4891 (2015).
31. M. Kawashiro, T. Mori, M. Ito, N. Ando, S. Yamaguchi, Photodissociative Modules that Control Dual-Emission Properties in Donor–π–Acceptor Organoborane Fluorophores. *Angew. Chem. Int. Ed.* **62**, e202303725 (2023).
32. Y. Wang *et al.*, A Multi-responsive System Based on Intramolecular B ← O=P Lewis Acid–Base Pairs. *J Mater Chem C* **10**, 10981-10987 (2022).
33. M. Gray, B. J. Chapell, J. Felding, N. J. Taylor, V. Snieckus, The di-tert-butylphosphinyl directed ortho metalation group. Synthesis of hindered dialkylarylphosphines. *Synlett*, 422-424 (1998).

34. D. Cinčić, T. Friščić, W. Jones, Experimental and database studies of three-centered halogen bonds with bifurcated acceptors present in molecular crystals, cocrystals and salts. *CrystEngComm* **13**, 3224-3231 (2011).
35. A. Bondi, van der Waals volumes and radii. *J. Phys. Chem.* **68**, 441-451 (1964).
36. E. Niecke, A. Fuchs, M. Nieger, Valence Isomerization of a 1,3-Diphosphacyclobutane-2,4-diyl: Photochemical Ring Closure to 2,4-diphosphabicyclo[1.1.0]butane and Its Thermal Ring Opening to gauche-1,4-Diphosphabutadiene. *Angew. Chem. Int. Ed.* **38**, 3028-3031 (1999).
37. A. Rodriguez *et al.*, Evidence for the coexistence of two bond-stretch isomers in solution. *Angew. Chem. Int. Ed.* **43**, 4880-4883, S4880/4881-S4880/4819 (2004).
38. L. Greb, Valence Tautomerism of p-Block Element Compounds – An Eligible Phenomenon for Main Group Catalysis? *Eur. J. Inorg. Chem.* **2022**, e202100871 (2022).
39. W. D. Stohrer, R. Hoffmann, Electronic structure and reactivity of strained tricyclic hydrocarbons. *J. Am. Chem. Soc.* **94**, 779-786 (1972).
40. W. D. Stohrer, R. Hoffmann, Bond-stretch isomerism and polytopal rearrangements in $(CH)_5^+$, $(CH)_5^-$, and $(CH)_4CO$. *J. Am. Chem. Soc.* **94**, 1661-1668 (1972).
41. F. A. Cotton, Discovering and understanding multiple metal-to-metal bonds. *Acc. Chem. Res.* **11**, 225-232 (1978).
42. R. F. W. Bader, *Atoms in Molecules: A Quantum Theory*. (Clarendon Press, Oxford, 1994), pp. 438 pp.
43. M. Baya, Ú. Belío, A. Martín, Synthesis, Characterization, And Computational Study of Complexes Containing Pt···H Hydrogen Bonding Interactions. *Inorg. Chem.* **53**, 189-200 (2014).
44. X. Wang, Q. Li, S. Scheiner, Cooperativity between H-bonds and tetrel bonds. Transformation of a noncovalent C···N tetrel bond to a covalent bond. *Phys. Chem. Chem. Phys.* **25**, 29738-29746 (2023).
45. J. S. Murray, P. Lane, T. Clark, K. E. Riley, P. Politzer, σ-Holes, π-holes and electrostatically-driven interactions. *J. Mol. Model.* **18**, 541-548 (2012).
46. P. R. Spackman *et al.*, CrystalExplorer: a program for Hirshfeld surface analysis, visualization and quantitative analysis of molecular crystals. *J. Appl. Crystallogr.* **54**, 1006-1011 (2021).
47. V. A. Pistritto, M. E. Schutzbach-Horton, D. A. Nicewicz, Nucleophilic Aromatic Substitution of Unactivated Fluoroarenes Enabled by Organic Photoredox Catalysis. *J. Am. Chem. Soc.* **142**, 17187-17194 (2020).
48. K. Tanaka *et al.*, Redox Potential Controlled Selective Oxidation of Styrenes for Regio- and Stereoselective Crossed Intermolecular [2 + 2] Cycloaddition via Organophotoredox Catalysis. *Org. Lett.* **22**, 5207-5211 (2020).
49. K. Tanaka *et al.*, Moderately Oxidizing Thioxanthylium Organophotoredox Catalysts for Radical-Cation Diels–Alder Reactions. *J. Org. Chem.* **87**, 3319-3328 (2022).
50. H. Kotani, K. Ohkubo, S. Fukuzumi, Photocatalytic Oxygenation of Anthracenes and Olefins with Dioxygen via Selective Radical Coupling Using 9-Mesityl-10-methylacridinium Ion as an Effective Electron-Transfer Photocatalyst. *J. Am. Chem. Soc.* **126**, 15999-16006 (2004).
51. S. Fukuzumi, K. Ohkubo, Organic synthetic transformations using organic dyes as photoredox catalysts. *Org. Biomol. Chem.* **12**, 6059-6071 (2014).
52. N. A. Romero, D. A. Nicewicz, Organic Photoredox Catalysis. *Chem. Rev.* **116**, 10075-10166 (2016).

53. K. A. Margrey, D. A. Nicewicz, A General Approach to Catalytic Alkene Anti-Markovnikov Hydrofunctionalization Reactions via Acridinium Photoredox Catalysis. *Acc. Chem. Res.* **49**, 1997-2006 (2016).
54. W.-C. Liu, F. P. Gabbaï, Placing Gold on a π^+-Surface: Ligand Design and Impact on Reactivity. *Chem. Sci.* **14**, 277-283 (2023).
55. P. Wawrzyniak, A. L. Fuller, A. M. Z. Slawin, P. Kilian, Intramolecular Phosphine−Phosphine Donor−Acceptor Complexes. *Inorg. Chem.* **48**, 2500-2506 (2009).
56. L. C. Wilkins, Y. Kim, E. D. Litle, F. P. Gabbaï, Stabilized Carbenium Ions as Latent, Z-type Ligands. *Angew. Chem. Int. Ed.* **58**, 18266-18270 (2019).
57. L. F. Tietze, C. Eichhorst, T. Hungerland, M. Steinert, A Fast Way to Fluorescence: A Fourfold Domino Reaction to Condensed Polycyclic Compounds. *Chem. Eur. J.* **20**, 12553-12558 (2014).
58. G. R. Fulmer *et al.*, NMR Chemical Shifts of Trace Impurities: Common Laboratory Solvents, Organics, and Gases in Deuterated Solvents Relevant to the Organometallic Chemist. *Organometallics* **29**, 2176-2179 (2010).
59. G. M. Sheldrick, *SADABS, Version 2007/4, Bruker Analytical X-ray Systems, Inc., Madison, Wisconsin, USA*. (2007).
60. G. M. Sheldrick, SHELXT - integrated space-group and crystal-structure determination. *Acta Crystallogr. A* **71**, 3-8 (2015).
61. G. M. Sheldrick. (Bruker Analytical X-ray Systems Inc., Madison, Wisconsin, USA, 2000).
62. D. M. Peloquin *et al.*, Spectroelectrochemistry of tris(bipyridyl)silicon(iv): ligand localized reductions with potential electrochromic applications. *Dalton Trans.* **44**, 18723-18726 (2015).
63. F. Neese, F. Wennmohs, U. Becker, C. Riplinger, The ORCA quantum chemistry program package. *J. Chem. Phys.* **152**, 224108 (2020).
64. A. V. Marenich, C. J. Cramer, D. G. Truhlar, Universal Solvation Model Based on Solute Electron Density and on a Continuum Model of the Solvent Defined by the Bulk Dielectric Constant and Atomic Surface Tensions. *J. Phys. Chem. B* **113**, 6378-6396 (2009).
65. R. Dennington, T. A. Keith, J. M. Millam. (Semichem Inc., Shawnee Mission, KS, 2019).
66. T. Lu, F. Chen, Multiwfn: A multifunctional wavefunction analyzer. *J. Comput. Chem.* **33**, 580-592 (2012).
67. T. A. Keith. (TK Gristmill Software, Overland Park KS, USA, 2014).
68. R. E. Abbott, *Symmetrical intramolecular substitution reactions. Models for a penta-coordinate carbon*. Department of Chemistry (Columbia University, 1972).
69. D. T. Hogan, T. C. Sutherland, Modern Spin on the Electrochemical Persistence of Heteroatom-Bridged Triphenylmethyl-Type Radicals. *J. Phys. Chem. Lett.* **9**, 2825-2829 (2018).
70. M. A. Spackman, J. J. McKinnon, Fingerprinting intermolecular interactions in molecular crystals. *CrystEngComm* **4**, 378-392 (2002).